THE JOURNAL OF PHYSICAL CHEMISTRY Letters

Letter

pubs.acs.org/JPCL

Resistive Pulse Delivery of Single Nanoparticles to Electrochemical Interfaces

Kim McKelvey, Martin A. Edwards, and Henry S. White*

Department of Chemistry, University of Utah, Salt Lake City, Utah 84112, United States

Supporting Information

ABSTRACT: An experimental system for controlling and interrogating the collisions of *individual* nanoparticles at electrode/electrolyte interfaces is described. A nanopipet positioned over a 400 nm radius Pt ultramicroelectrode is used to deliver individual nanoparticles, via pressure-driven solution flow, to the underlying electrode, where the nanoparticles undergo collisions and are detected electrochemically. High-velocity collisions result in elastic collisions of negatively charged polystyrene nanospheres at the Pt/water interface, while low-velocity collisions result in nanoparticle adsorption ("sticky" collisions). The ability to position the nanopipet with respect to the underlying ultramicroelectrode also allows the time between particle release from the nanopipet and electrode collision to be investigated as a function of nanopipet−electrode separation, d. The time between release and collision of the nanoparticle is found to be proportional to d^3, in excellent agreement with an analytical expression for convective fluid flow from a pipet orifice.

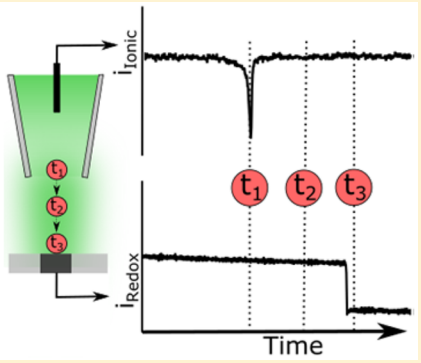

The collision of single nanoparticles with electrode surfaces is of fundamental interest in nanoscale electrochemistry, potentially providing a wealth of information about parameters that determine nanoparticle electrocatalytic activity.[1,2] In a typical nanoparticle collision experiment, the transient changes in electrochemical current resulting from metal particle collisions that catalyze a redox reaction are recorded as a function of time. These experiments are generally performed in solutions containing a relatively high density of nanoparticles, e.g., 10^8 cm^{-3}; thus, the electrochemical signals reflect the behavior of a large ensemble of events that correspond to various particle shapes and sizes. In addition, nanoparticle collision experiments rely on the stochastic diffusion-driven transport of nanoparticles from the bulk solution to the electrode surface that cannot be easily controlled. Thus, a demand exists for techniques that can control the delivery of individual nanoparticles to electrode interfaces.[3,4]

Herein, we offer a proof of principle demonstration of a combination electrochemical measurement that allows both particle size measurement and controlled delivery of nanoparticles to electrochemical (and other) interfaces. Two techniques, resistive pulse sensing (RPS)[5,6] and the nanoparticle collision method,[1,7] are performed simultaneously, allowing complementary measurements of individual nanoparticles as well as control of the nanoparticle-electrode collision dynamics. The technique, which is illustrated schematically in Figure 1, uses a nanopipet containing nanoparticles positioned above an ultramicroelectrode (UME) in solution for pressure-controlled delivery of single nanoparticles. Each single particle passing through the nanopipet orifice generates a resistive pulse; this resistive pulse serves two purposes in our experiment: (1) it indicates the precise time when a particle is emitted from the orifice, which is required for investigating motional dynamics, and (2) it can be used to estimate the size of the particle via classical resistive pulse theory, where the pulse peak height is proportional to the particle volume.[5] Following particle emission from the pipet, and after a time delay that varies with distance between the pipet orifice and electrode surface, collision of the nanoparticle with the electrode is detected electrochemically through a change in the redox current. In the experiments reported here, a small Pt disk electrode is used as the delivery target to detect nanoparticle collisions. In principle, any collision interaction that generates a change in the electrochemical response of the target electrode can be used to measure particle arrival and the transport dynamics of the particle between the pipet and electrode. In this Letter, we demonstrate the method by delivery of nonelectroactive polystyrene particles that cause a change in the electrochemical response of the Pt disk electrode, either by transiently passing through the depletion layer or sticking to the surface. We show that the probability of a "sticky" collision can be controlled using the pipet delivery system.

In the combined RPS−collision experiment (Figure 1, detailed in section S2 of the Supporting Information) the pipet is filled with an aqueous electrolyte solution containing 241 ± 3 nm radius polystyrene nanoparticles (see section S1 of the Supporting Information for a scanning electron micrograph of nanoparticles), a redox mediator (2 mM FcMeOH), 5 mM NaCl, 0.5 mM K_2HPO_4, and 0.005 vol % Triton X-100 solution in ultrapure water from a Barnstead Smart2Pure water

Received: August 19, 2016
Accepted: September 20, 2016
Published: September 20, 2016

DOI: 10.1021/acs.jpclett.6b01873
J. Phys. Chem. Lett. 2016, 7, 3920−3924

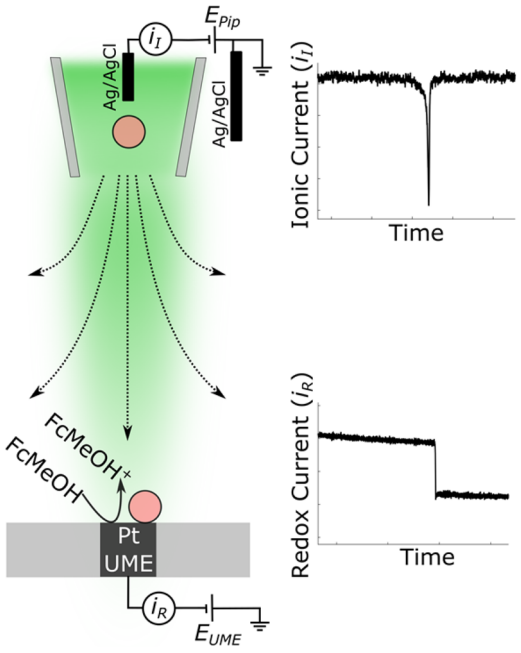

Figure 1. Schematic of a combined resistive pulse sensing−particle collision experiment, with the relative size of the nanopipet opening (700 nm radius), polystyrene nanoparticles (241 nm radius), Pt UME (405 nm radius), and nanopipet−UME distance (5 μm) drawn to scale. The nanopipet contains polystyrene nanoparticles and redox mediator (FcMeOH) in buffer (indicated as green shading), and the external solution contains only buffer. The ionic current (i_I), measured at the Ag/AgCl electrode inside the nanopipet, and the redox current (i_R), measured at the ultramicroelectrode, are recorded simultaneously. A positive pressure is applied to the nanopipet to drive the convective flow of solution/nanoparticles from the nanopipet, illustrated as convective flow lines out of the nanopipet.

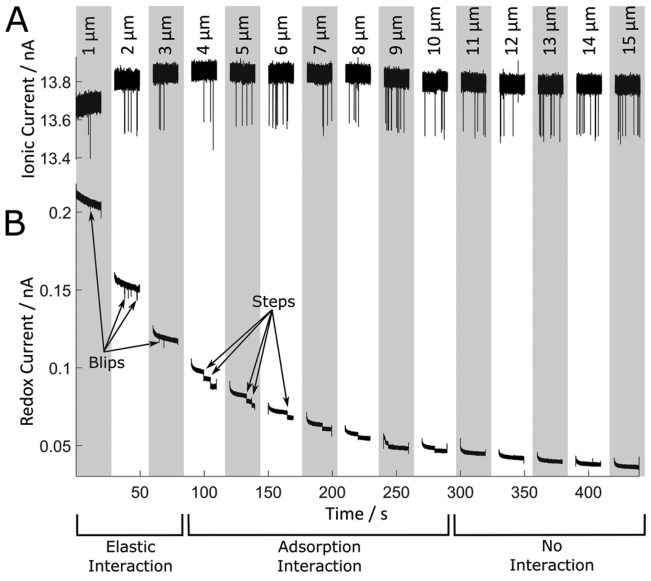

Figure 2. (A) Ionic current traces and (B) concurrent redox current traces with the nanopipet at a series of different nanopipet−UME distances (1−15 μm) above the 405 nm Pt UME, showing the delivery of single 241 nm polystyrene nanoparticles. Data were recorded at E_{UME} = 0.4 V for 30 s at each height, followed by potential reversal to −0.5 V for 10 s to desorb any particles from the interface. Additional data collected with a different pipet on a different day is presented in section S11 of the Supporting Information and displayed similar behavior.

purification system (Thermo Scientific) with a resistivity of 18.2 MΩ cm at 25 °C. The external solution contains the same electrolyte solution, but without particles or redox mediator. Positioning of the pipet precisely above the UME was achieved in a two-step procedure detailed in section S3 of the Supporting Information. Briefly, approximate positioning was achieved using manual micropositioners while the position was monitored through orthogonally mounted cameras. Subsequent precise positioning was achieved using piezo actuators and ionic current feedback. The ionic current (i_I) between a Ag/AgCl electrode inside the pipet and an identical one in bulk solution was used to monitor the pipet−surface separation while the redox current (i_R) caused by "collection" (oxidation) of FcMeOH exiting the pipet (green in Figure 1) was used for lateral positioning; the nanopipet was deemed to be centered over the electrode when a maximum redox current was obtained (section S3 of the Supporting Information).

With the pipet centered over the electrode, a small pressure (1 ± 0.5 mmHg) was applied to the pipet to slowly drive particles into the external solution, while the pipet was positioned at successively greater distances from the electrode surface. The ionic and redox current−time traces acquired simultaneously during this experiment are shown in Figure 2. The ionic current (top trace) shows resistive pulses (momentary drops in ionic current), each corresponding to a single nanoparticle exiting the nanopipet. The background ionic current is relatively constant at different probe−substrate distances, except at the very closest nanopipet−UME distances, which is consistent with scanning ion current microscopy results for a pipet of this size (700 nm).[8,9] The asymmetric shape of the resistive pulses, which can be seen on an expanded time scale in Figure 3, arises from the conical shape of the pore.[10] The magnitude of the resistive pulses (2 ± 0.2%) is constant over nanopipet−UME distance and also consistent with resistive pulse measurements in bulk solution (section S4 of the Supporting Information). Because the particles are highly monodisperse (section S1 of the Supporting Information), we primarily attribute the variability in the amplitude of the resistive pulses to the intrinsic variability in the resistive pulse technique.[11]

The corresponding redox current at the Pt UME, which was simultaneously acquired, is shown as the lower curve in Figure 2. The current was recorded while the electrode potential (E_{UME}) was poised at 400 mV, a potential sufficient for mass-transport limited oxidation of FcMeOH. Abrupt changes in redox current, either "elastic" interactions (*blips* or transient decreases in current followed by a return to baseline) or adsorption interactions (*steps* or a permanent decrease in current), are indicative of the interaction of single nanoparticles with the underlying UME (vide infra) and were not observed in the absence of nanoparticles. What is referred to as an elastic collision in this context is not a true momentum-conserving collision, but a collision in which the attractive electrostatic forces adhering the nanoparticle to the surface are less than the convective kinetic forces acting on the nanoparticle, resulting in a transient interaction with the electrode surface. In the intervening times when moving the pipet (see section S5 of the Supporting Information for data), the electrode (E_{UME}) was poised at −500 mV for 10 s, which is sufficient to electrostatically drive any adsorbed PS nanoparticles from the surface (see section S6 of the Supporting Information). Figure

DOI: 10.1021/acs.jpclett.6b01873
J. Phys. Chem. Lett. 2016, 7, 3920−3924

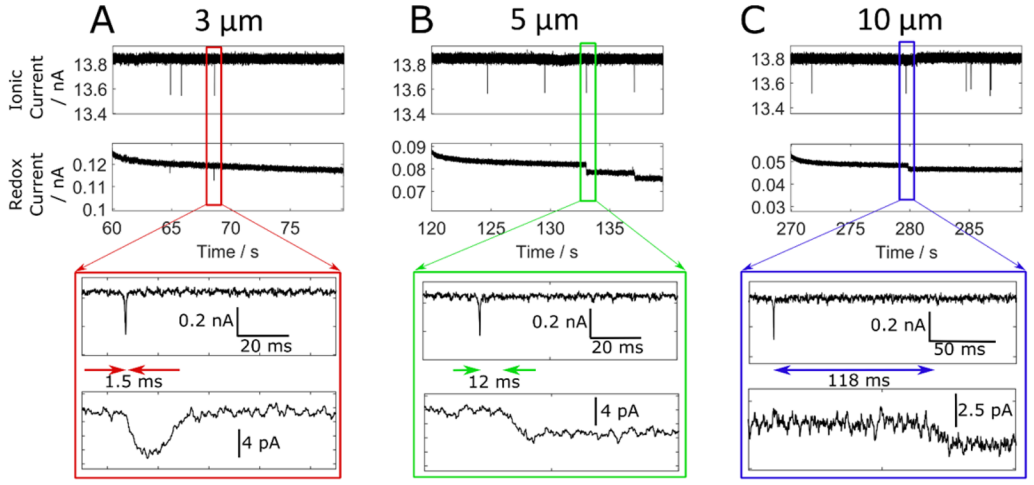

Figure 3. Current−time traces for both the ionic current and redox current with the nanopipet positioned 3 μm (A), 5 μm (B), and 10 μm (C) above the UME. (Current−time traces for all distances are available in section S7 of the Supporting Information).

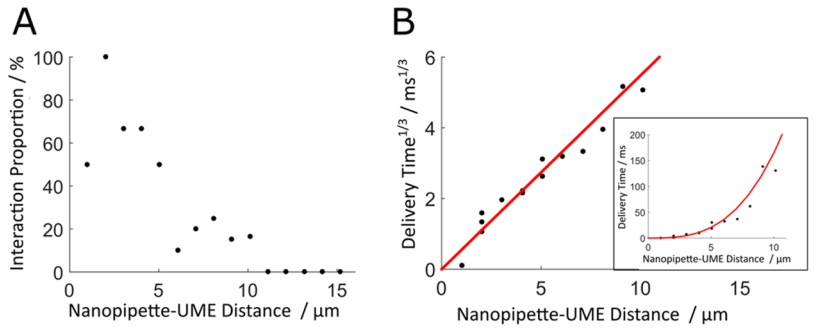

Figure 4. (A) Proportion of delivered nanoparticles interacting with the underlying UME (either elastic or adsorption response) as a function of the nanopipet−UME separation. (B) Cube root of the delay between the nanoparticle exiting the nanopipet (maximum of resistive pulse) and its interaction with the UME as a function of nanopipet−UME distance. Particles that did not interact were not included in this analysis. Shown in red is the line of best fit. Inset shows plot of nanopipet−UME distance vs delivery time.

2 shows that there is a decreasing background redox current with increasing nanopipet−UME separation, which is consistent with the source of FcMeOH (pipet) being steadily moved further from the electrode.

Typical examples of the elastic and adsorption behaviors are shown on an expanded scale in Figure 3 (see section S7 of the Supporting Information for further examples). The step response due to particle adsorption is consistent with results from particle collision experiments in which nanoparticles were added to the unstirred bulk solution with a uniform concentration of redox mediator (section S6 of the Supporting Information);[12] the step decrease in redox current is due to the particle permanently attaching (electrostatically) to the electrode and hindering diffusion of the mediator. The magnitude of the step in redox current was computed from finite element simulations and is a function of the relative size of the nanoparticle relative to the size of the underlying UME (in this case, 241 nm/405 nm ≈ 0.6) and its location on the surface.[13,14] An average redox current blockage of 3.5 ± 1% is experimentally observed, which is lower than the average redox current blockage of 6 ± 2% that we observe in bulk measurements in stagnant bulk solution (see section S4 of the Supporting Information) and also lower than would be expected from previous measurements[12] and finite element simulations, also in stagnant solutions (section S8 of the Supporting Information). This suggests that the nonuniform FcMeOH distribution, as well as the effects of fluid convection, slightly reduce the effect of the particle blocking transport of FcMeOH to the Pt electrode. This can be simulated using finite element methods for a quantitative determination of the redox current blockage, but is beyond the scope of this work.

The elastic collision response can be attributed to a nanoparticle passing in close proximity to the electrode and temporarily blocking the flux of FcMeOH. Finite element simulations indicate that the redox current blockage responses for a particle briefly touching the electrode and a particle coming in close proximity to the Pt UME cannot easily be distinguished by the magnitude of the redox current blockage (section S8 of the Supporting Information).

Interestingly, elastic responses were observed for pipet−electrode separations of 3 μm and less, while at a separation between 4 and 10 μm, absorption responses are uniquely observed (Figure 2), a point discussed in more detail below. In replicate experiments, such as is shown in section S11 of the Supporting Information, the pipet−electrode separation at which elastic and absorption responses were observed differed slightly and were not always unique (i.e., at some distances both inelastic collision and absorption responses are observed). The diffusion-limited redox current for the oxidation of FcMeOH at the Pt UME was monitored between experiments and did not change. This indicates stability of the Pt UME.[15] We ascribe the variability in elastic and absorption response to slight differences in the pipet and UME alignment and small differences in the applied pressure.

DOI: 10.1021/acs.jpclett.6b01873
J. Phys. Chem. Lett. 2016, 7, 3920−3924

Not all resistive pulses are accompanied by a corresponding change of the redox current at the Pt electrode, as can be observed in Figure 3. From this we are confident that the Pt electrode response is not a result of the nanoparticle blocking the flow of redox species out of the nanopipet. The proportion of nanoparticles exiting the pipet that resulted in a response at the UME (elastic or absorption) is plotted in Figure 4A, demonstrating that at larger nanopipet−UME separation, the nanoparticle is less likely to be detected at the underlying UME. This behavior is consistent with convective transport of nanoparticles from the nanopipet to a relatively small UME over a large distance, with only the nanoparticles passing through the very center of the nanopipet orifice having a significant probability of collision with the Pt UME.

Inspection of the current−time traces shown on expanded scales in Figure 3 indicates that the ionic and redox current responses are not concurrent. The redox current response is observed after the resistive pulse with a delay that increases with nanopipet−UME distance, a relationship that is plotted in Figure 4B. The delay shows very little stochasticity, which is consistent with transport of nanoparticles from the nanopipet to the UME being dominated by convection. At the smallest nanopipet−UME distance (1 μm), we observe the resistive pulse is nearly coincident (within ~1 ms) with the drop in redox current at the Pt UME, indicating that the 241 nm radius nanoparticle is blocking the flux of mediator to the UME even as it passes through the end of the nanopipet.

A detailed understanding of the transport from nanopipet to electrode involves considering details of the fluid flow as well as diffusional (Brownian) motion. The pressure driven flow in a conical nanopipet is parabolic in nature with a volumetric flow rate given by[16]

$$Q = 3\pi r_0^3 \Delta p / 8\eta \cot\theta \quad (1)$$

with a maximum flow rate $v_{max} = 2Q/\pi r_0^2$ obtained at the center of the orifice.[17] In our experiments, r_0 = 700 nm is the nanopipet radius, $\Delta p = 1 \pm 0.5$ mmHg the applied pressure, η the viscosity (set to 1×10^{-3} Pa), and θ the nanopipet cone angle (set to 10°), which give $Q = 1 \pm 0.5 \times 10^{-14}$ m^3/s and $v_{max} = 1.3 \pm 0.6 \times 10^{-2}$ m/s. N.B.: Imprecision in values arises from limited precision in pressure measurement.

In bulk solution and at moderate distances from the orifice, the fluid velocity is spherically symmetric and decreases with the square of the distance from the orifice, r;[18,19] i.e, the radial component of the velocity can be described by

$$v(r) = Q/4\pi r^2 \quad (2)$$

While a complete description of the flow would require numerical simulations, such as those for an impinging jet,[20,21] and is beyond the scope of this work, a fair approximation of the delivery time, t, can be obtained through assuming the particle follows a radial streamline and integrating the analytical expression for v^{-1} from eq 2

$$t = \int v^{-1} \mathrm{d}r = (4\pi/3Q) r^3 \quad (3)$$

Experimental data show an excellent fit to a cubic relation (red line in Figure 4B) which gives a volumetric flow $Q = 2.5 \pm 0.3 \times 10^{-14}$ m^3/s (equivalently $v_{max} = 3.3 \pm 0.6 \times 10^{-2}$ m/s). This value compares well with the flow rate calculated from eq 1 ($Q = 1 \pm 0.5 \times 10^{-14}$ m^3/s, $v_{max} = 1.3 \pm 0.6 \times 10^{-2}$ m/s) with uncertainty in the pipet geometry, contributions of electroosmosis to flow, and nonspherical flow close to the pipet orifice and surface all possible sources of the small discrepancy.

The Peclet number, $Pe = dv/D$, describes the ratio of convection to diffusion in mass-transport, where d is a characteristic length, D the diffusion coefficient, and v the velocity. $Pe \ll 1$ indicates that diffusional transport dominates, while $Pe \gg 1$ indicates that convection dominates. For a 241 nm radius nanoparticle $D = 8.9 \times 10^{-13}$ m^{2}s^{-1} (Stokes−Einstein), and we set d equal to the radius of the UME, 405 nm. Note that because of divergent streamlines, only nanoparticles that pass (approximately) through the center of the orifice ultimately collide with the relatively small UME.

While $Pe \approx 1900$ at the opening of the nanopipet indicates transport is dominated by convection, the velocity, and hence Pe, drops with the distance from the orifice. Assuming eq 2, at a distance of 10 μm from the orifice $Pe \approx 10$ and diffusional transport begins to contribute significantly to mass transport. Beyond this distance nanoparticle collisions with the electrode become highly unlikely as random diffusion takes the nanoparticle off the streamlines directing it at the UME. Note that this analysis of Pe validates our use of a deterministic calculation of delivery time above.

By delivering single nanoparticles from a nanopipet to an underlying UME, we have demonstrated that two simple electrochemical methods for the detection of single nanoparticles, the resistive pulse sensing method and the particle collision method, can be combined to provide complementary measurements of an individual nanoparticle. We exploit this and show how we can control the delivery and capture of nanoparticles using the convective flow out of the nanopipet. This method could be extended using our newly developed multipass resistive pulse methods to provide more precise size[10,22] and shape characterization[23] of the particles delivered. Finally, although demonstrated with inert monodisperse polystyrene nanoparticles, this method can be extended to polydisperse metal nanoparticles, allowing single nanoparticle size and electrocatalytic activity to be measured.

■ ASSOCIATED CONTENT

Supporting Information

The Supporting Information is available free of charge on the ACS Publications website at DOI: 10.1021/acs.jpclett.6b01873.

Scanning electron microscopy of nanoparticles, experimental details, nanopipet positioning details, resistive pulse detection of individual polystyrene nanoparticles in bulk solution, full traces for the delivery and detection of single nanoparticles at different heights, detection of polystyrene nanoparticles from bulk solution at a Pt-UME, current−time traces at different nanopipet−UME distances, finite element simulations, fabrication of nanopipets and determination of their size, determination of electrode size, replicate combined RPS−nanoparticle collision experiments (PDF)

■ AUTHOR INFORMATION

Corresponding Author

*E-mail: white@chem.utah.edu.

Notes

The authors declare no competing financial interest.

DOI: 10.1021/acs.jpclett.6b01873
J. Phys. Chem. Lett. 2016, 7, 3920−3924

■ ACKNOWLEDGMENTS

This work was funded by Air Force Office of Scientific Research MURI FA9550-14-1-0003. We thank Dr. Qianjin Chen for the Pt-UME fabrication and Mr. Sean German and R. Polson for assistance with scanning electron microscopy. This work made use of University of Utah shared facilities of the Micron Technology Foundation Inc. Microscopy Suite sponsored by the College of Engineering, Health Sciences Center, Office of the Vice President for Research, and the Utah Science Technology and Research (USTAR) initiative of the State of Utah.

■ REFERENCES

(1) Rees, N. V. Electrochemical Insight from Nanoparticle Collisions with Electrodes: A Mini-Review. *Electrochem. Commun.* **2014**, *43*, 83−86.
(2) Murray, R. W. Nanoelectrochemistry: Metal Nanoparticles, Nanoelectrodes, and Nanopores. *Chem. Rev.* **2008**, *108*, 2688−2720.
(3) Kleijn, S. E. F.; Lai, S. C. S.; Miller, T. S.; Yanson, A. I.; Koper, M. T. M.; Unwin, P. R. Landing and Catalytic Characterization of Individual Nanoparticles on Electrode Surfaces. *J. Am. Chem. Soc.* **2012**, *134*, 18558−18561.
(4) Wang, Y.; Cai, H.; Mirkin, M. V. Delivery of Single Nanoparticles from Nanopipettes under Resistive-Pulse Control. *ChemElectroChem* **2015**, *2*, 343−347.
(5) Luo, L.; German, S. R.; Lan, W.-J.; Holden, D. A.; Mega, T. L.; White, H. S. Resistive-Pulse Analysis of Nanoparticles. *Annu. Rev. Anal. Chem.* **2014**, *7*, 513−535.
(6) Coulter, W. H. Means for Counting Particles Suspended in a Fluid. U.S. Patent 2656508, 1953.
(7) Cheng, W.; Compton, R. G. Electrochemical Detection of Nanoparticles by "nano-Impact" Methods. *TrAC, Trends Anal. Chem.* **2014**, *58*, 79−89.
(8) Chen, C.; Zhou, Y.; Baker, L. A. Scanning Ion Conductance Microscopy. *Annu. Rev. Anal. Chem.* **2012**, *5*, 207−228.
(9) Edwards, M. A.; Williams, C. G.; Whitworth, A. L.; Unwin, P. R. Scanning Ion Conductance Microscopy: A Model for Experimentally Realistic Conditions and Image Interpretation. *Anal. Chem.* **2009**, *81*, 4482−4492.
(10) Edwards, M. A.; German, S. R.; Dick, J. E.; Bard, A. J.; White, H. S. High-Speed Multipass Coulter Counter with Ultrahigh Resolution. *ACS Nano* **2015**, *9*, 12274−12282.
(11) Qin, Z.; Zhe, J.; Wang, G.-X. Effects of Particle's off-Axis Position, Shape, Orientation and Entry Position on Resistance Changes of Micro Coulter Counting Devices. *Meas. Sci. Technol.* **2011**, *22*, 045804.
(12) Quinn, B. M.; van 't Hof, P. G.; Lemay, S. G. Time-Resolved Electrochemical Detection of Discrete Adsorption Events. *J. Am. Chem. Soc.* **2004**, *126*, 8360−8361.
(13) Fosdick, S. E.; Anderson, M. J.; Nettleton, E. G.; Crooks, R. M. Correlated Electrochemical and Optical Tracking of Discrete Collision Events. *J. Am. Chem. Soc.* **2013**, *135*, 5994−5997.
(14) Boika, A.; Thorgaard, S. N.; Bard, A. J. Monitoring the Electrophoretic Migration and Adsorption of Single Insulating Nanoparticles at Ultramicroelectrodes. *J. Phys. Chem. B* **2013**, *117*, 4371−4380.
(15) Nioradze, N.; Chen, R.; Kim, J.; Shen, M.; Santhosh, P.; Amemiya, S. Origins of Nanoscale Damage to Glass-Sealed Platinum Electrodes with Submicrometer and Nanometer Size. *Anal. Chem.* **2013**, *85*, 6198−6202.
(16) Lan, W.-J.; Holden, D. A.; Liu, J.; White, H. S. Pressure-Driven Nanoparticle Transport across Glass Membranes Containing a Conical-Shaped Nanopore. *J. Phys. Chem. C* **2011**, *115*, 18445−18452.
(17) Giddings, J. C. *Unified Separation Science*; Wiley: New York, 1991.
(18) Kirkpatrick, D. C.; Edwards, M. A.; Flowers, P. A.; Wightman, R. M. Characterization of Solute Distribution Following Iontophoresis from a Micropipet. *Anal. Chem.* **2014**, *86*, 9909−9916.
(19) Uitto, O. D.; White, H. S.; Aoki, K. Diffusive-Convective Transport into a Porous Membrane. A Comparison of Theory and Experiment Using Scanning Electrochemical Microscopy Operated in Reverse Imaging Mode. *Anal. Chem.* **2002**, *74*, 4577−4582.
(20) Macpherson, J. V.; Marcar, S.; Unwin, P. R. Microjet Electrode: A Hydrodynamic Ultramicroelectrode with High Mass-Transfer Rates. *Anal. Chem.* **1994**, *66*, 2175−2179.
(21) Bitziou, E.; Rudd, N. C.; Edwards, M. A.; Unwin, P. R. Visualization and Modeling of the Hydrodynamics of an Impinging Microjet. *Anal. Chem.* **2006**, *78*, 1435−1443.
(22) German, S. R.; Hurd, T. S.; White, H. S.; Mega, T. L. Sizing Individual Au Nanoparticles in Solution with Sub-Nanometer Resolution. *ACS Nano* **2015**, *9*, 7186−7194.
(23) Zhang, Y.; Edwards, M. A.; German, S. R.; White, H. S. Multipass Resistive-Pulse Observations of the Rotational Tumbling of Individual Nanorods. *J. Phys. Chem. C* **2016**, DOI: 10.1021/acs.jpcc.6b02018.

DOI: 10.1021/acs.jpclett.6b01873
J. Phys. Chem. Lett. 2016, 7, 3920−3924